Springer

KSME

Journal of Mechanical Science and Technology 24 (11) (2010) 2347~2355
www.springerlink.com/content/1738-494x
DOI 10.1007/s12206-010-0617-8

Heat transfer performance of condenser tubes in an MSF desalination system †

T. Galal*, A. Kalendar, A. Al-Saftawi and M. Zedan

Department of Mechanical Engineering, College of Technological Studies, Public Authority for Applied Education & Training
P.O. Box 42325, Shuwaikh, 70654, Kuwait

(Manuscript Received May 6, 2009; Revised Febraury 16, 2010; Accepted June 19, 2010)

Abstract

The present research examines the amount of condensed fresh water off the outer-side surface of heat exchangers in an MSF system. The quantitative modeling of condensed water on the outer surface of comparable tubes, enhanced and plain, in a simulated MSF technique is investigated. An adapted simulation design on a test-rig facility, accounting for the condenser tubing in actual industrial desalination plate-form, is used with corrugated and smooth aluminum-brass material tubes 1100mm long and 23mm bore. A single-phase flow of authentic brine water that typifies real fouling is utilized to simulate the actual environmental life of a multi-stage flashing desalination system, with coolant flow velocity 0.1 m/s in the two delineated types of condenser tubing. It is demonstrated that the condensate water amount from the specified enhanced tube is about 1.22 times the condensate water amount from the smooth tube, adaptive for 140 running hours under deliberated constrains. The topic covers a comparative analysis of thermal performance. Comparing results with fresh water confirm the effect of fouling on significantly lowering the value of the overall heat transfer coefficient versus time. Fouling resistance R_f is reported with the critical coolant flow speed of 0.1 m/s. Comparison between the fouling resistance for both smooth and corrugated tubes versus time is performed. The fouling thermal resistance of the corrugated tube is 0.56 of the fouling thermal resistance of the smooth tube after140 running hours of the experiment are concluded. Overall, in the case of real brine, results prove that heat performance for the corrugated tube is superior to the plain tube over the studied time period (140 hrs) for the chosen range of flow speeds.

Keywords: Desalination; MSF system; Condenser; Smooth tube; Corrugated tube

1. Introduction

Desalination stations in Kuwait are integrated with electrical power plants, Fig. 1 [1, 2]. The series of heat exchangers used by Multi-Stage Flashing (MSF) units is composed of classical smooth tubes, with each unit producing distillate water in millions of imperial gallons per day. As the MSF system experiences severe mechanical difficulties due to fouling in the condenser tubing, approaches were made to improve the system's thermal efficiency. A continuous cleaning system known as ball cleaning Fig. 2 [3] is used to overcome the fouling problem. Also, an interesting approach is being proposed to use enhanced tubes to improve heat transfer performance in an MSF system. The current study is primarily concerned with the enhancement of MSF performance when replacing a smooth tube with a corrugated one. They are supposed to have different characteristics in terms of heat transfer and pressure drop. Specifications of the tube are highlighted in Fig. 3 [4, 5]. Fig. 3.1 depicts a photograph of the tube like the one used in the current research, while Fig. 3.2 and Table 1 shows the associated dimensions.

When a corrugated tube is used, the expectations are increased production of desalinated water and/or decreases in required

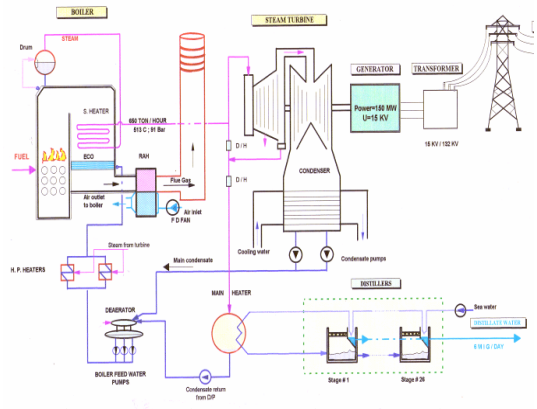

Fig. 1. Doha East Power and Desalination Station [2].

† This paper was recommended for publication in revised form by Associate Editor Man-Yeong Ha

* Corresponding author. Tel.: +965 9 716 7761, Fax: +965 2 481 1753
E-mail address: trgalal70@hotmail.com

© KSME & Springer 2010

Table 1. Dimensional properties of Wolverine Korodense tube.

Tube length, L=1100 mm	Corrugation depth, e= 0.58 mm
Outer diameter, D_o = 25.4 mm	Internal diameter, D_i = 23 mm
Helix angle β relative to the axis of the tube	Number of starts, n_s=1
The axial corrugation pitch, p = 10.64 mm	$p = \frac{\pi d_i}{n_s \tan \beta}$

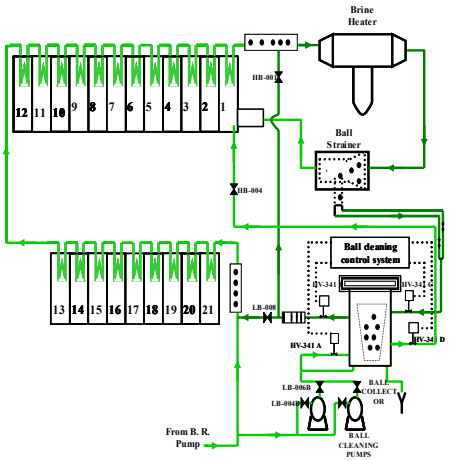

Fig. 2. Ball cleaning system [3].

Fig. 3.1. Photograph of Wolverine Korodense tube [4].

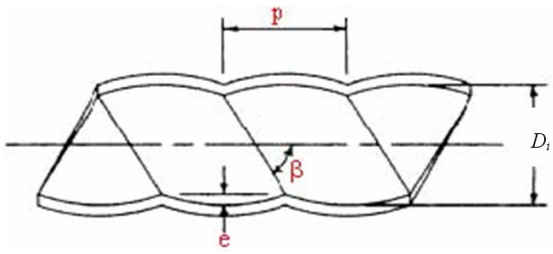

Fig. 3.2. Diagram of Wolverine Korodense tube [5].

pumping power [6]. Heat transfer and enhancement of heat exchangers were examined by several researchers [7], while most of the fouling research was conducted with single-phase flow in a smooth tube [8]. Fouling and enhancement were investigated separately with little cross-referencing of the two. Kim & Webb [9], and Charm & Webb [10] concluded that the thermal performance of an enhanced tube remains superior to the plain tube in spite of a higher fouling (a particulate fouling) data rate recorded on the former. Because fouling is a slow process, most of the research was conducted in a laboratory using a highly concentrated particulate artificial fouling in order to get results within several hours or several days. This has led to unambiguous experimental data when comparing enhanced heat transfer surface performance to the plain surface.

Fouling from natural brine water is unlike artificial fouling, since it involves more than one category of fouling, which is difficult to deal with. It is not possible to address this kind of difficulty in most research programs. Thus, any change to the operating characteristics needs to be balanced by the gains and off-set against its time dependent performance. Hence, the vital link between surface heat transfer rate and problems associated with fouling over such enhanced surfaces needs to be explored so that a fundamental understanding of the relationship of the two can be analyzed [11], while ref. [12-14] studied the influence of flow speed and tube diameter on fouling resistance.

The approach of the current research is to assess the feasibility of an enhanced heat transfer mechanism in MSF plants by comparing the collected quantity of condensate water to the amount collected with a smooth tube. Using a corrugated tube transfers the mode of water accumulation on the outer-side of the tube surface from a film-wise to drop-wise condensation, potentially increasing the amount of condensed water collected. In addition, actual brine water that typifies real process conditions was used. The performance of the enhanced tube combined with the existence of fouling was examined with an emphasis on whether more water was accumulated [15].

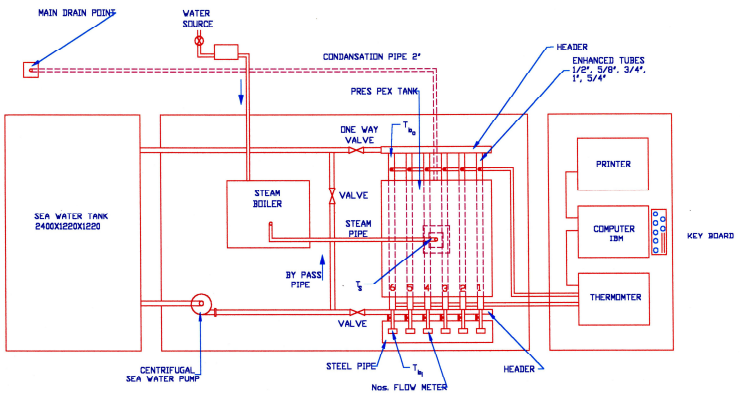

Fig. 4.1. A horizontal plan of the experimental set-up.

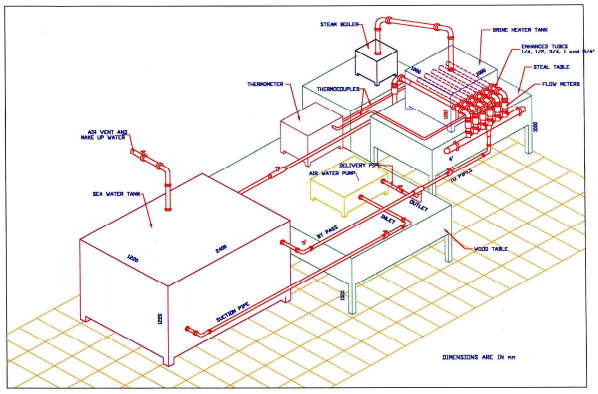

Fig. 4.2.1. Experimental layout, with a cubic box test-rig (a first design configuration).

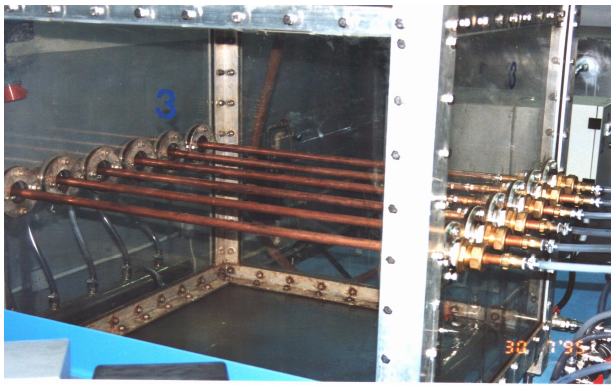

Fig. 4.2.2. A photograph of the cubic box rig.

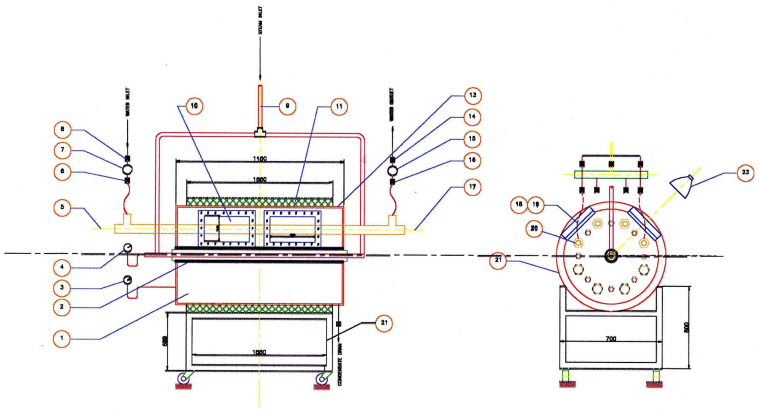

Fig. 4.3. Schematic of test rig [12, 13].

2. Test rig

A horizontal plan for the experimental set-up is given in Fig. 4.1. An isometric lay-out of the experimental facilities with a cubic box test rig, with availability for testing six tubes at a time (as a first design configuration) and a common header for both inlet and outlet tubes, is given in Fig. 4.2,. A cylindrical drum test rig was developed due to the failure of the former design by buckling and cracking of the Plexiglass box's wall (12 *mm* thickness) by thermal stresses. A schematic drawing is shown on Fig. 4.3, with separate inlet and outlet headers for each tube. The system consists mainly of a condenser with the availability to test eight tubes at a time, a boiler, a brine circulating pump, a brine storage tank, measuring instruments, data acquisition system, and a computer.

Figs. 5 and 6 show photos of the main components of the rig-facilities. The test rig uses a condenser with a 78 *cm* di-

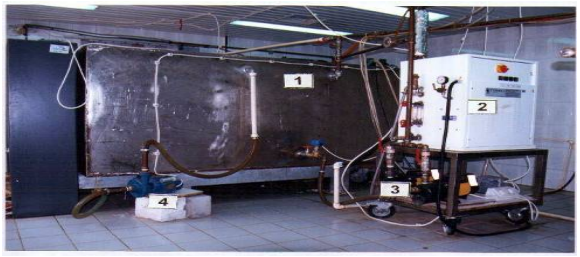

1	Brine water storage tank.
2	Steam boiler.
3	Brine water circulating pumps.
4	Cooling brine water feed pump.

Fig. 5. Main components of test rig facilities [12].

ameter and a length of 110 *cm*. The drum frame is designed using stainless steel 316 in two shells with outer and inner thicknesses of 2 *mm*, with thermal insulation provided in between for the purpose of minimizing heat dissipation. Four windows are built into the upper half of the considered shelled frame using a heat resistant glass (up to700℃) of a 6 *mm* thickness to help in observing the developments inside the condenser during the experiment. Tested tubes are distributed inside the drum on an equal circular pitch angle. The rig design is capable of testing eight tubes at a time, as shown in Fig. 4.3, providing better circumstances for obtaining similarity and symmetry. Steam is introduced to the cylindrical condenser through two central entrances.

The steam distributor tubing inside the condenser consists mainly of two overlapped tubes. The inner tube is designed to scatter the steam, whereas the outer one is built-in for the purpose of avoiding the creation of a steam jet by distributing the steam uniformly throughout the condenser. To measure the steam temperature inside the cylindrical condenser, four thermo-couples are built into the rig—two on the upper half and two on the lower half. Through this arrangement, it has been proved that the steam temperature is distributed uniformly throughout the rig "T_{srig}". The temperature is taken as almost constant throughout the experiments. T_{srig} is adapted by controlling the steam supply valve. Used thermocouples are chosen to be capable of withstanding corrosive media while covering the required range of measured temperatures.

The brine-circulating pump used in this test is a compact single-stage jet-assisted centrifugal pump with a mechanical shaft seal and "o" ring casing seal. The pump provides reliable higher pressures at flows of 35 *lpm*. It is manufactured from quality corrosion-resistant materials, quickly and easily installed, requires low maintenance, and is easy to service. Its capacity is 35 *lpm* @ 140 *kpa*, with a maximum total head of 35 *m*. A vortex flow meter is used. The meters are fitted on the downstream of the condenser.

The flow rates are measured electronically using accurate vortex shedding technology. Through the data acquisition system, data readings (temperature, pressures, and flow rates)

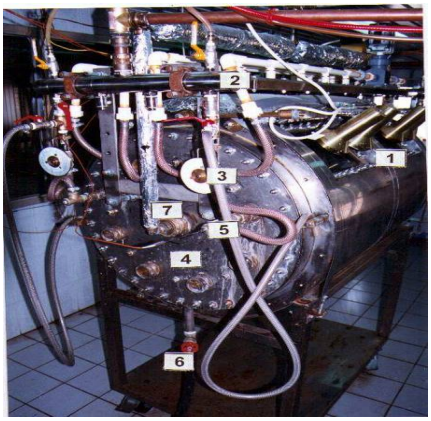

	A lighted glass window
2	An outlet header
3	An outlet control valve
4	A backside tube opening flange
5	A thermocouple
6	A condensate drain valve
7	A backside steam inlet

Fig. 6.1. An overall back view of test rig (B) [12].

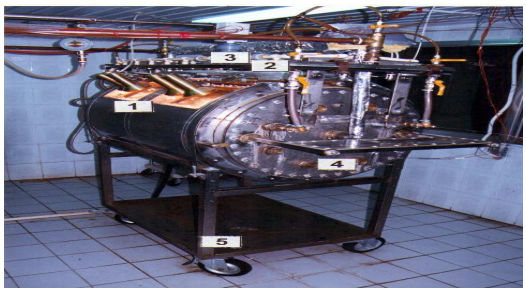

1	Alighted glass window
2	An inlet header
3	A flow meter
4	A front side opening
5	A stand

Fig. 6.2. Overall front view of test rig (B).

are to record every specified time interval onto the computer hard disk and a printer output. The test rig was instrumented in such a way that temperature at all important points in the apparatus (inlet and outlet of each tube and the boiler outlet) can be monitored, as well as the flow rate of all the fluid streams. Moreover, the measurement and control system is used to take the required temperature automatically as programmed. In addition, the provided software package allows the user to write his own algorithm to optimize the system for a particular application.

Thermocouples are inserted into the important points where

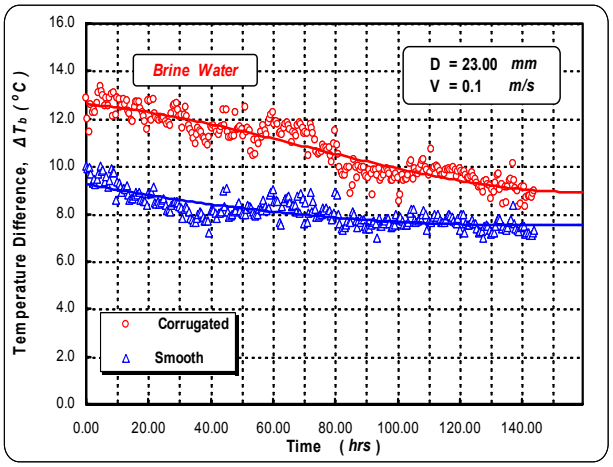

Fig. 7. Variation of temperature difference (ΔT_b) with time, for corrugated and smooth tubes.

temperatures are to be recorded. E-type thermocouples are connected to the measurement and control link units via a card containing 9 channels. Each thermocouple is calibrated and connected to a channel in this card. There is one channel for boiler outlet, one for the tube inlets, and one for each tube outlet.

3. Experiment data set

In the current research, two Al-Brass tubes are used for testing: a corrugated tube, C, and a smooth tube, S, with diameter 23 mm as given in Appendix (A). Brine-water passes through these tubes at speed of 0.1 m/s. An electric boiler is utilized to supply the distributor tubing inside the condenser with a saturated water vapor. Steam and brine inlet and outlet temperatures are measured. To define utilized measurement accuracy Appendix (B) displays the uncertainty analysis. Fig. 7 shows brine coolant temperature rise (ΔT_b) between inlet and outlet) change for both tubes versus time. Temperature rise for corrugated tube is higher than smooth tube by 37% at t =0, reduced to an asymptotic value of 19% after 144 hrs.

4. Data correlation & results

In a heat exchanger, with one fluid a saturated vapour and the other a brine coolant, the applied heat transfer equation is given by:

$$Q = U\ A_i\ \theta_m\ kW \tag{1}$$

U is the overall heat transfer coefficient, A_i is the nominal inside surface area, and θ_m is the logarithmic mean temperature difference. The logarithmic mean temperature difference, θ_m, on Fig. 8 is given by:

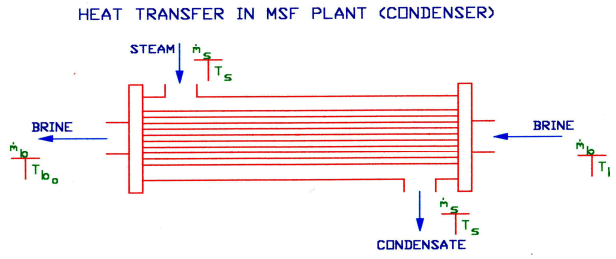

Fig. 8. Tubing of an MSF plant's condenser.

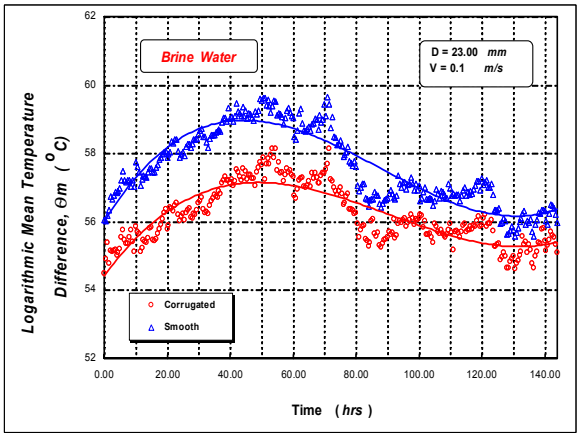

Fig. 9. Variation of θ_m for both tubes versus time.

$$\theta_m = \frac{T_{bo} - T_{bi}}{Ln\left[\frac{T_s - T_{bi}}{T_s - T_{bo}}\right]}\ ^oC \tag{2}$$

The brine water inlet temperature, T_{bi}, is not constant due to circulation. It has been realized that the measured vapor temperature in the drum is lower than the saturation temperature at the stage operating pressure (atmospheric), owing to its blending with exerted gases, accompanied by the expansion and cooling processes of mixture as it flows around the tubes. In calculating θ_m, the value of the steam temperature T_s is taken equal to T_{srig}, the actual drum steam temperature. Recorded readings of T_{srig} versus time are given in Table A-1 for the first 10 hours.

Calculated values of θ_m for both tubes on 144 hours are illustrated on Fig. 9. There are two observations worth mentioning on this graph. First, values of θ_m for the smooth tube are higher than those of the corrugated tube. Second, values of θ_m for both tubes increased with time to a certain maximum, then decreased, with this trend extended to certain asymptotic values. Curves fluctuated with long periods according to the definition of θ_m given by Eq. (2). The variation of ΔT_b with time is shown on Fig. 7, while Table A-1 shows the first 10 hours of experimentally recorded data for both smooth and corrugated tubes, showing measurement differences between the steam-side and seawater-side.

Table 2. Typical 1 is for stage 19 of heat gain section-plant No.1 – Doha East* [2]., while Current 2 is for our corrugated tube data.

Parameters	Typical 1	Current 2	Parameters	Typical 1	Current 2
Pipe Type Material	Smooth Al-brass	corrugated Al-brass	T_{bi} ℃	46.3	34.8
Pipe Length (m)	17.7	1.1	T_{bo} ℃	47.5	43.6
Pipe D_i (mm)	36.88	23	ΔT ℃	1.2	8.8
Fluid Vel. m/s	2.08	0.1	T_s ℃	50.2	100
U kW/m^2 ℃	1.7	0.36	θ_m ℃	3.26	56.2

* Data collected on: July 19 & 20, 1978

$$Q = m_b\, C_p\,(T_{bo} - T_{bi}) = m_b\, C_p\, \Delta T_b \;\; kW \tag{3}$$

Comparison of present measurements for the overall heat transfer coefficient with the correlation data collected is given in Table 2, showing a huge difference in U values between actual field-site design data and our current experimental data. This is due to the vast difference in θ_m values for a same given heat transfer rate Q. Table 2 shows θ_m actual within 3.26° C, due to the narrow range of ΔT chosen for the given stage 1.2℃, while the steam saturation temperature would be in a range of 2 degrees higher than the brine water coolant outlet temperature of 50.2℃. These design arrangements are adapted to reduce the value of θ_m and maximize U values. In our current experiment, these arrangements are not taken into consideration, since it is not within the scope of our research.

The heat transfer rate through the tested tube using the brine water side of the energy balance is given by the following Equations:

The collected experimental data are used to determine the overall heat transfer coefficient vs. time through Eqs. (1), (2), and (3) for a certain considered nominal inside surface area A_i of a tube. U can be given by (1) as:

$$U = \frac{Q}{A_i\, \theta_m} \;\; kW/m^2 \tag{4}$$

A_i is the nominal inside surface area (m^2), $A_i = \pi D_i L$, D_i is the tube's inner diameter *(m)*, and L is the tube's length (*m*). Fig. 10 describes the variation of the overall heat transfer coefficient for both tubes versus time. As shown on the figure, the values of U for both tubes decrease with time due to tube fouling. However, the value of U for the corrugated tube is superior to the smooth tube during the test. U for the corrugated tube is at least 1.3 times that of the smooth tube.

Based on the assumption that the steam side energy is balancing the sea water side heat energy, Q in Eq. (4) can be determined using the steam side energy as follows:

$$Q = m_w\, h_{fg} \;\; kW \tag{5}$$

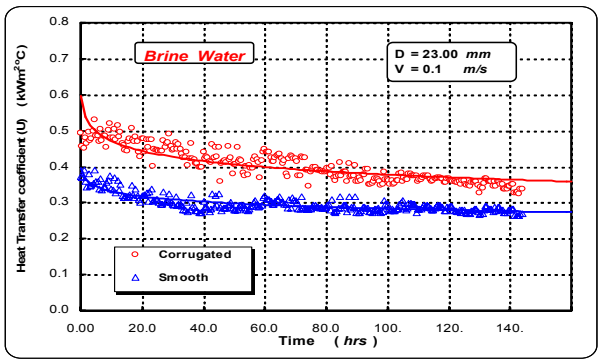

Fig. 10. Variation of the overall heat transfer coefficient (U) with time for corrugated and smooth tubes (23.0 mm diameter, 0.1 m/s flow velocity).

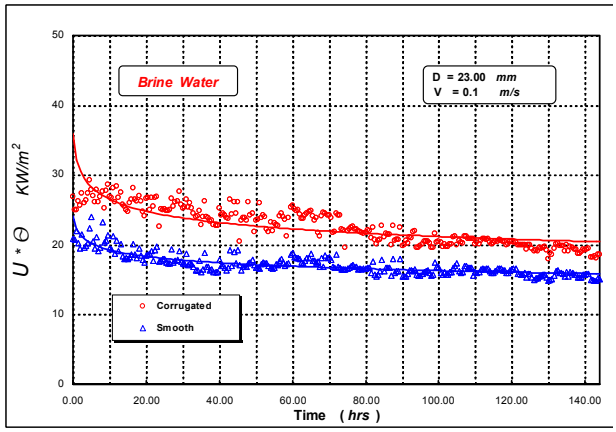

Fig. 11. Variation of ($U * \theta_m$) for both tubes versus time.

m_w = The rate of mass condensed water on each external tube surface (kg/s)

h_{fg} = The steam enthalpy of condensation (kJ/kg)

From the formulas given above and Eq. (3), the following correlation is defined:

$$\frac{m_{w,c}}{m_{w,s}} = \frac{U_c\;\; \theta_{m,c}}{U_s\;\; \theta_{m,s}} = \frac{m_b\, C_p \left(\Delta T_{b,c}\right)}{m_b\, C_p \left(\Delta T_{b,s}\right)} \tag{6}$$

$m_{w,c}$ is the rate of condensation by the corrugated tube (c), while $m_{w,s}$ is the rate of condensation by the smooth tube (s). Eq. (6) gives the ratio for the given tubes. As seen by the equation, this can be determined by the ratios of $U * \theta_m$ or by the ratios of ΔT_b for both tubes. *Brine water* ρ and C_p are functions of temperature given in Eqs. A1 and A2, Appendix (A). Results show insignificant variation of ρ and C_p with temperature. Therefore, the term ($m_b\, C_p$) in Eq. (6) is assumed to be identical for both tubes.

Fig. 11 records the variation of ($U * \theta_m$) for both tubes versus time. As shown, the ($U * \theta_m$) values of the corrugated tube are higher than those of the smooth tube.

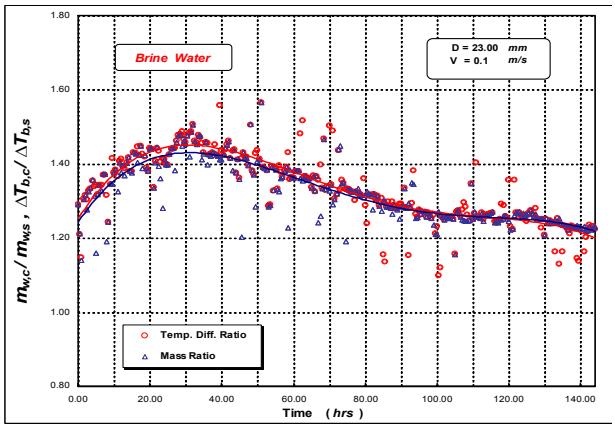

Fig. 12. The condensate mass ratio ($m_{w,c}/m_{w,s}$) versus time.

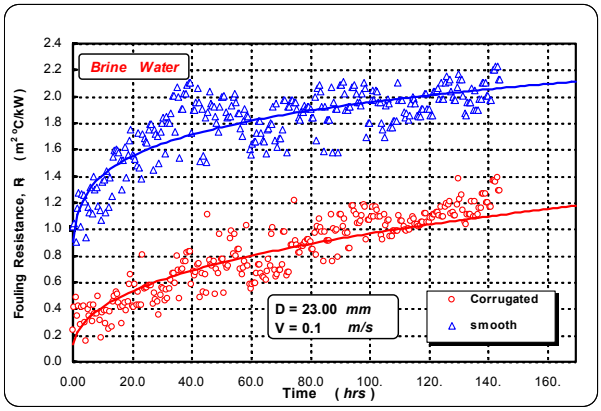

Fig. 13. Fouling resistance (R_f) for both tubes versus time.

Fig. 12 shows the undergoing change of condensate mass ratio $m_{w,c}/m_{w,s}$ versus time, illustrating that the rate of condensation from the corrugated tube is more significant. Therefore, the amount of condensate water collected out of the specified enhanced tube, under deliberated constrains, is at least 1.22 times the condensate amount given out by the smooth tube. Also, it shows a slight difference between the ratios of $(U*\theta_m)$ and (ΔT_b) due to neglected variations in ρ and C_p.

Fouling resistance is typically performed by measuring the total thermal resistance $(1/UA_i)$ for clean and fouled cases (Webb [13]) using the following formula:

$$\frac{R_f}{A_i} = \frac{1}{(UA_i)_f} - \frac{1}{(UA_i)_{cl}} \quad {}^oC/kW \tag{7}$$

Where subscript *f* and *cl* refer to fouled and clean conditions. The results for fouling resistance (R_f) of both corrugated and smooth tubes are illustrated in Fig. 13. As shown, the fouling thermal resistance for both tubes increases with time then attains a somewhat constant asymptotic value after 144 hours. This happens when the solid deposition rate and the rate of removal reach an equal value. The figure also shows that the performance for the corrugated tube is superior to that of the smooth tube. Fouling thermal resistance of the smooth tube is 1.77 of that for the corrugated tube. It is worth mentioning that the current work test rig ran for 3-4 hours before starting recording results. This is may explain the given values of R_f for both tubes at t=0.

5. Conclusions

A research test-rig is used to simulate the heat exchange process in an actual desalination plant. Simulation of actual circumstances in real desalination plate-form is done, with tube constituents: aluminum-brass material, 23 mm diameter, 1100mm length**;** employing authentic brine water with a critical coolant flow speed of 0.1 m/s. The following is resolved: the amount of condensate water from the specified enhanced tube, under deliberated constrains is at least 1.22 times the amount of condensate water from the tested smooth tube, adaptive for 140 experimental running hours. In other words, the accomplished data proved that corrugated tube heat performance is superior to the performance of smooth tube for a given tube size and the investigated coolant speed, where heat rate improvement is interpreted as energy saving.

Results for fouling resistance R_f are presented with the same velocity value chosen (0.1 m/s) to describe the case, since it is comprehended from experimental trials that fouling resistance is the highest on this reported low speed. A comparison between fouling resistance for both smooth and corrugated tubes versus time is done, confirming that the smooth tube has a higher fouling tendency than that of the corrugated tube. Concluded results show that the fouling thermal resistance of the corrugated tube is 0.56 of fouling thermal resistance of the smooth tube.

Future work should include experimental investigation with a simulated design on a test rig to verify the collected quantitative amount of water condensation out of the comparable tubes**;** re-examination of the accumulated water collected out of same type of corrugated tube, but with different corrugation pitch and depth; experimentation with other tube geometries, types of enhancement, and other classes of tube materials, e.g. copper-Nickel (Cu-Ni), in order to optimize the tube data results.

Acknowledgment

This work has been financially supported by PAAET; project No.TS-08-11, yr. 2009. This support is gratefully acknowledged.

Nomenclature

A : Considered area for heat transfer, m^2
A_i : Nominal inside surface area, m^2
C_P : Specific heat of brine, kJ/kg °
h_{fg} : Steam enthalpy of condensation, kJ/kg
R_f : Fouling thermal resistance, m^2 °C/kW
m_b : Mass flow rate of brine, kg/s
m_w : Mass of condensed water on external tube surface, kg/s

$m_{w,c}$: Rate of water mass condensed by corrugated tube (c)
$m_{w,s}$: Rate of water mass condensed by smooth tube (s)
U : Overall hear transfer coefficient, kW/ m^2 ºC
T_{bi} : Brine temp. at the entrance to the condenser, ºC
T_{bo} : Brine temp. at the exit from the condenser, ºC
$T_{bo,c}$: Brine water outlet temp. from the corrugated tube, ºC
$\Delta T_{b,c}$: Temp. difference for corrugated tube, $(T_{bo,c} - T_{bi})$, ºC
$T_{bo,s}$: Brine water outlet temp. from the smooth tube, ºC
$\Delta T_{b,s}$: Temp. difference for smooth tube, $(T_{bo,s} - T_{bi})$, ºC
T_{sboil} : Steam outlet temperature from boiler, ºC
T_{srig} : Steam temperature inside the test-rig, ºC
T_s : Steam temp. value used in calculation of θ_m = 100ºC
T_{bi} : Brine temperature in, ºC
θ_m : Logarithmic mean temperature difference, ºC
D_i : Tube inside diameter, m
L : Tube length, m
Q : Heat flux, kW

References

[1] T. H., J. E., W. T. H. and J. C., A Short Course on: Desalination Technology, *King Abdul-Aziz University*, Jeddah, Saudi Arabia, March (1980).
[2] Private communications, *Training Department, Doha east power & water production station, ministry of electricity & water*, Kuwait.
[3] Private communications, *Training Department, Doha east power & water production station, ministry of electricity & water*, Kuwait.
[4] J. R. Thome, *Engineering Data Book III*, Wolverine Tube Inc. (2008).
[5] Wolverine Tube Guide, *Wolverine Tube Inc. Decatur*, Alabama 53609-2202, USA.
[6] Private communication, *Wolverine Tube Inc.*, Huntsville AL35801, USA.
[7] A. E. Bergles, Techniques to Augment Heat Transfer-second-Generation Heat Transfer Technology, *Journal of Heat Transfer*, (110) (1985) 1082-1096.
[8] A. P. Watkinson, Fouling of Augmented Heat Transfer Tubes, *Heat Transfer Engineering*, 11 (3) (1990) 57.
[9] N. H. Kim and R. L. Webb, Particulate Fouling of Water in Tubes Having Two Dimensional Roughness Geometry, *Int. J. Heat Mass Transfer*, 34 (11) (1991) 2727.
[10] L. M. Chamra and R. L. Webb, Modelling Liquid-Side Particulate Fouling in Enhanced Tubes, *Int. J. Heat Mass Transfer*, 37 (4) (1994) 571.
[11] D. L. Gee and R. L. Webb, Forced Convection Heat Transfer in Helically Rib-Roughened Tubes, *International Journal of Heat Mass Transfer,* 23 (1980) 1127-1136.
[12] A. Y. Kalendar An Investigation of Scale Depositing on Enhanced Distillation Heat Transfer Tube Surfaces, *Ph.D. Thesis*, Cardiff University (2000).
[13] A. Y. Kalendar and A. J. Griffiths, Performance Study of Enhanced and Smooth Surface Tubes in a System Condenser of a Multistage Flash Desalination Unit, *ELSEVIER; Desalination Journal* 134 (2000) 269-283.
[14] R. L. Webb,. *Principle of Enhanced Heat Transfer*, John Wiley & Sons, Inc. (1994).
[15] T. Galal, A. Kalendar, A. Al-Saftawi and M. Zedan, Condensate Water Quantity Function of Condenser Tubing Type for Innovation MSF System, *ADST Proceedings*, International Conference Desalination Technologies and Water Reuse, May 7-8 (2007).
[16] Albright & Wilson, Water Management Chemicals-Desalination Technical Service, *Albright & Wilson U.K. Limited*, U.K.

Appendix (A)

A.1 Primary data sheet

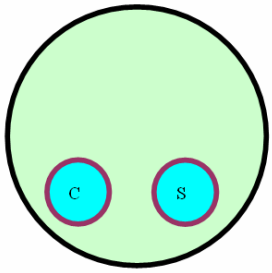

Test No. 13

Tube dia. = 23m

Water type	*Brine*
Tube cross sec. area A_{in}	0.0004153 m^2
Tube Surface area	0.079442 m^2
Water density	1.027 kg/lit

	Tube c*	Tube s
Tube Material	Al. Brass	Al. Brass
Flow Vel. m/sec	0.0985	0.0993

* The letter (c) is taken as a subscript to presents the corrugated tube, while the letter (s) is for the smooth tube

Above data sheet and the following table show that the volume flow rate in both tubes are about the same, however, both tubes have different characteristics in terms of heat transfer and pressure drop.

Table A.1. The experimentally recorded data sheet for smooth and corrugated tubes.

Time (hrs)	$T_{bo,c}$ ℃	$T_{do,s}$ ℃	$dT_{bo,c}$ ℃	$dT_{bo,s}$ ℃	T_{srig} ℃	T_{bi} ℃	T_{sboil} ℃
0	47.606	44.707	12.884	9.985	95.915	34.722	100.474
0.5	46.807	44.726	11.987	9.906	95.933	34.82	100.486
1	46.156	44.686	11.421	9.951	96.031	34.735	100.506
1.5	47.236	44.287	12.602	9.653	95.946	34.634	100.479

2	46.629	43.693	12.245	9.309	95.892	34.384	100.375
2.5	46.662	43.782	12.361	9.481	95.834	34.301	100.411
3	46.675	43.65	12.264	9.239	95.909	34.411	99.339
3.5	46.845	43.681	12.646	9.482	95.944	34.199	99.213
4	47.182	43.744	13.105	9.667	95.897	34.077	100.369
4.5	47.505	44.122	13.384	10.001	96.173	34.121	100.419
5	47.303	43.955	13.128	9.78	96.188	34.175	99.293
5.5	46.91	43.794	12.95	9.834	96.227	33.96	100.3
6	46.378	43.181	12.521	9.324	96.121	33.857	100.343
6.5	46.908	43.614	12.881	9.587	96.177	34.027	100.354
7	46.744	43.361	12.527	9.144	96.065	34.217	100.32
7.5	46.87	43.397	12.852	9.379	96.058	34.018	100.308
8	46.91	43.794	13.006	9.89	96.207	33.904	100.287
8.5	46.436	44.06	12.113	9.737	96.35	34.323	100.383
9	47.257	43.9	13.103	9.746	96.378	34.154	100.331
9.5	47.138	43.575	12.156	8.593	96.408	34.982	100.337
10	46.717	43.202	12.866	9.351	96.387	33.851	100.351

A.2 Brine water properties [16]

Density "ρ"

The density of sea water can be calculated using the following formula, derived from Grunberg, using Tschebyscheff polynomials [14]:

$$\rho = \{1/2\, a_0 + a_1 Y + a_2 (2Y^2 - 1) + a_3 (4Y^3 - 3Y)\} \qquad \text{(A1)}$$

Where,

$a_0 = 2.016110 + 0.115313\, Z + 0.000326\, (2Z^2 - 1)$

$a_1 = -0.054100 + 0.001571\, Z - 0.000423\, (2Z^2 - 1)$

$a_2 = -0.006124 + 0.001740\, Z - 0.000009\, (2Z^2 - 1)$

$a_3 = 0.000346 + 0.000087\, Z - 0.000053\, (2Z^2 - 1)$

$Y = (2T - 200)/160, \quad Z = (2S - 150)/150$

The density is calculated in $gram/cm^3$, T is in ^0C and S (salinity) in g/kg. {For condensate water; Z = -1, since $S = 0$}.

The specific heat capacity "C_p".

The specific heat capacity of seawater is calculated by the following formula, as quoted [14]:

$$C_p = (A + BT + CT^2 + DT^3) \qquad kJ/kg\,^0C \qquad \text{(A2)}$$

Where,

$A = 4206.8 - 6.6197\, S + 1.2288 * 10^{-2} S^2$

$B = -1.1262 + 5.4178 * 10^{-2} S - 2.2719 * 10^{-4} S^2$

$C = 1.2026 * 10^{-2} - 5.3566 * 10^{-4} S + 1.8906 * 10^{-6} S^2$

$D = 6.8774 * 10^{-7} + 1.5170 * 10^{-6} S - 4.4268 * 10^{-9} S^2$

With T as the average temperature across the heat recovery section in ℃, and S as the salinity of brine in g/kg.

Appendix (B)

B.1 Uncertainty analysis for inlet coolant temperature

To estimate the uncertainty for the coolant inlet temperature as an example to define our measurement accuracy, a method presented by Kline and McClintock is used. The method is based on the uncertainties in various primary experimental measurements such as flow rate and temperature. The estimation of the uncertainty in calculated results depends on the accuracy of basic measurements.

In this study, the result, R, is given as a function of independent variable, x. Thus,

$$R = R(x)$$

Let W_r be the uncertainty in the result, and W_1 be the uncertainty in the coolant inlet temperature as an independent variable. The calculated uncertainty is expressed as:

$$W_r = [\partial R/\partial x]\, W_1$$

The basic uncertainty reference value W_1 for the independent variable under scope "T_{bi}" is: ± 0.1 to 0.2
Recalling Eq. 4:

$$U_i = \frac{m_b C_P}{A} \ln\left[\frac{T_s - T_{bi}}{T_s - T_{bo}}\right], \quad kW/m^2\,^oC \qquad \text{(B1)}$$

With,

$A = 5.56 \times 10^{-2}\ m^2$, T_{b_i} (portable)=20℃, T_{bi} (brine) = 25℃,
$T_s = 115$℃, $m_b = 0.522$ kg /min, and $C_p = 4.2$ kJ / kg ℃.

$$|\partial R/\partial x| \equiv |\partial U/\partial T_{bi}| = |\, m\, C_p / A\, (T_s - T_{bi})\,| \cong 0.03$$

$$W_r \cong 0.01$$

Tarek Galal received his B.S. degree in Mechanical Engineering from An Shams University, Cairo, Egypt, in 1973; his M. Eng. degree from McGill University, Montreal, Canada in 1982; and his Ph.D. from Franche-Comte Universite, France in 1989. He is currently a lecturer at the Department of Mechanical Engineering Technology at the Public Authority for Applied Education & Training in Kuwait.. His research interests are in the area of heat transfer and solar energy.